Effects of laminate thickness and reinforcement type on the impact behaviour of E-glass/polyester laminates

L. S. Sutherland and C. Guedes Soares

Abstract

A large number of impact tests have been carried out on woven-roving and chopped-strand-mat glass reinforced, hand laid-up polyester laminates of different thicknesses and weights. Deflection, force, absorbed energy and damaged area results for these tests have been presented and compared, and the failure modes described. A simple analysis assuming shear-dominated deflection gave good correlation with the experimental data. Prediction of the damaged area proved to be more difficult, although some correlation was seen. Further investigation into the nature of the damage is required.

Keywords

A. Polymer matrix composites
A. Glass fibres
A. Short-fibre composites
A. Textile composites
B. Impact behaviour

1. Introduction

Fibre-reinforced plastics (FRPs) are now an accepted material used in many and varied applications in different fields of engineering. Advantages that have contributed to the recent increase in the use of FRPs include their high specific strength and stiffness, the ease with which complex shapes may be formed and their chemical and environmental resistance, amongst others. However, a known weakness of these materials is their susceptibility to impact damage, especially transverse impact normal to the plane of the laminae. This potential weakness is due to the brittle nature of the reinforcing fibres, the lack of through thickness reinforcement and the relatively low interlaminar shear strengths of these materials.

The impact damage sustained usually consists of matrix cracking and degradation, surface microbuckling, fibre fracture and internal delamination. The exact nature of this damage is dependent upon the nature of the composite and of the test specimen, and also upon the test geometry and conditions. The damage mechanisms are highly complex and interactive due to the nature of the microstructure of these materials, and extremely difficult to model. A commonly used, practical assessment of the impact damage is the degradation in load-bearing capacity of the material after impact. Tensile and flexural testing after impact are carried out, but the property most affected by impact damage is usually compressive strength, and compression-after-impact (CAI) tests are most commonly used.

The reduction in compressive strength is mainly due to internal delamination, which may not be visible. This is a problem in that undetected impact damage may lead to an unexpected, and possibly catastrophic, failure at a later date if the impaired strength of the structure does not exceed an operational load. Also, the impact delamination may grow as a result of repeated loading or impact until the load-bearing capacity of the structure is lost.

Impact is an important issue in the marine industry because of the possibility of damage sustained during fabrication, for example the dropping of tools or collisions whilst moving or turning modules during assembly. Also, in-service damage may arise from regular minor impacts whilst docking, through the striking of floating objects in the water, to collisions with other vessels, and to grounding.

There is a wealth of literature on the impact behaviour of composite materials, and this literature covers many aspects of this complex composites testing area. Generally, however, the literature concentrates on expensive, high-quality, high-Vf carbon/epoxy laminates such as are commonly used in the aerospace industry. The incident kinetic energy is usually not thought to be sufficient to define the impact event, incident velocity [1] and the maximum force and absorbed energy histories are also found to be important [2,3]. The use of maximum impact force has been used with some success by Davies and Zhang [4] to normalise the results of impact tests on various specimen sizes, geometries and boundary conditions. The dominating failure mechanism is often internal shear delamination [5].

There is far less work concerning glass-fibre-reinforced plastics. By considering impact force and absorbed energy histories Zhou and Davies [6] predicted the onset of impact damage of woven-roving E-glass/polyester laminates of high fibre volume fraction. Shear delamination was assumed to model the damage area. In a previous paper, Sutherland and Guedes Soares [7] investigated the impact behaviour of low-V_f, hand laid-up E-glass-reinforced polyester laminates. The effects of specimen thickness (5 and 10 plies), impactor kinetic energy and impact velocity were investigated. Damage was observed for all impact energies. Different laminators were used to replicate the tests to look for operator effects, but these were not found to be large. The assumption that shear deformation dominates the response gave good agreement with the results. A model assuming a circular delamination area predicted very well the inter-laminar shear strength for the 5-ply specimens, but not for the 10-ply specimens.

This paper aims to extend the work already carried out concerning such composites to include the impact behaviour of equivalent laminates using both a heavier woven-roving (WR) and also chopped-strand-mat (CSM) reinforcements. The effect of thickness was also further investigated through the inclusion of 15-ply tests.

2. Experimental details

An instrumented falling-weight-impact test machine was used for the tests in this work. A controlled, repeatable impact is achieved by dropping a striker attached to a variable weight onto the sample in a defined manner and at a prescribed impact velocity. During the impact, the resistive force exerted by the specimen on the striker is measured by a load cell as a function of time, and stored for subsequent display and analysis. The software calculates, from the basic force–time information, velocity, distance and energy absorbed by the specimen.

There are three main parts to the falling-weight apparatus, a tower where the weight falls onto the sample held below, a control unit, and the computer software system. The tower consists of a sample area, where a pneumatic clamp holds the sample, and a column down which an impactor head attached to a weight falls onto the sample. The specimens were clamped using a 'picture frame' clamp of dimensions 120 mm by 75 mm with the flat, mould side of the specimen facing down.

Panels of 1 m by 1 m were laminated by hand on a horizontal flat mould, and after these panels had cured, rectangular specimens of 100 mm by 150 mm were cut out using a diamond-surrounded saw. For the woven-roving specimens the warp was aligned with the longer dimension.

The materials used were 500 and 800 gm^{-2} balanced woven-roving, and 450 gm^{-2} chopped-strand-mat E-glass and polyester resin cured using 1, 2 and 3% by weight of accelerator, catalyst and paraffin, respectively. The resin used was isopthalic for the 500 gm^{-2} woven-roving 5- and 10-ply specimens and orthopthalic for the rest of the specimens. The woven-roving and chopped-strand-mat laminates were nominally of 50 and 33% fibre weight fraction, respectively.

Panels of 5, 10 and 15 plies were laminated using the 500 gm^{-2} WR to view the effect of thickness on the impact behaviour. To investigate the effect of reinforcement weight, 800 gm^{-2} WR was also used, 3 and 6 plies giving the nearest equivalent to the 5- and 10-ply 500 gm^{-2} WR panels. To investigate the behaviour of a different form of reinforcement, 450 gm^{-2} CSM was used to fabricate 5- and 10-ply panels.

For the specimens from each panel tests were performed at eight increasing incident energy levels, at both the highest and lowest velocities attainable within the constraints of the test machine. One repetition of each test was made, giving 32 tests from each panel, and a total of 224 specimens.

The literature concerning carbon composites inspects the damage sustained by the specimens after impact using ultrasonic C-scan methods. However, the laminates considered here were translucent and it was possible to view the damage simply by backlighting the specimens. This gave the approximate damaged area, and also a qualitative description of the damage.

3. Results

The full results are given in the Appendix.

Table 1 compares the weights per square meter and average thicknesses of the laminates. The coefficients of variation of these thicknesses are also given. The ply weights were chosen to give as equivalent laminate weights as possible.

Table 1 shows that although these weights are close, the 800 gm^{-2} WR and 450 gm^{-2} CSM laminate are 4 and 10% lighter than the 500 gm^{-2} WR laminates, respectively. The thinner WR laminates are of the same average thickness, considering the variation in the data, but for the thicker specimens the 500 gm^{-2} WR laminate is, on average, slightly thicker (by 8%) the 800 gm^{-2} WR one. The CSM laminates are much thicker than the equivalent WR

laminates, and show a great deal of variation in these thicknesses because of the unstable nature of this reinforcement which makes controlled laminating difficult.

Laminate	Weight (gm^{-2})	Average thickness (mm)	Thickness coefficient of variation
5-Ply 500 gm^{-2} WR	2500	3.14	0.05
3-Ply 800 gm^{-2} WR	2400	3.10	0.06
5-Ply 450 gm^{-2} CSM	2250	5.12	0.15
10-Ply 500 gm^{-2} WR	5000	6.16	0.06
6-Ply 800 gm^{-2} WR	4800	5.70	0.04
10-Ply 450 gm^{-2} CSM	4500	10.57	0.09
15-Ply 500 gm^{-2}	7500	9.10	0.04

Table 1. Laminate weights and thicknesses

3.1. Damage and failure modes

3.1.1. WR specimens

The damage sustained by the woven-roving specimens may be grouped into three main categories; front-face buckling delamination under the impactor, internal shear delamination and back-face matrix and fibre degradation. The front-face and internal delaminations were approximately circular for lower impact energies, but became progressively mis-shapen as the severity of impact increased. The back-face damage consisted of a central area of matrix cracking and progressive degradation, and then associated fibre damage and failure at medium and high energies, respectively. As the highest energies were reached, failure occurred either in the form of varying degrees of perforation of the specimen by the impactor, or by a line of shear failure from the centre of the specimen to the centre of the long edge of the clamp.

Generally the thinner laminates retain the damage characteristic of low-energy impacts up to energies closer to their final failure than do the thicker specimens. That is, similar trends in impact damage may be seen as the impact energy is increased or as the specimen thickness is increased. This is perhaps not surprising as the thicker laminates are subjected to higher impact energies. Typical damage modes are shown in Figs. 1 and 2.

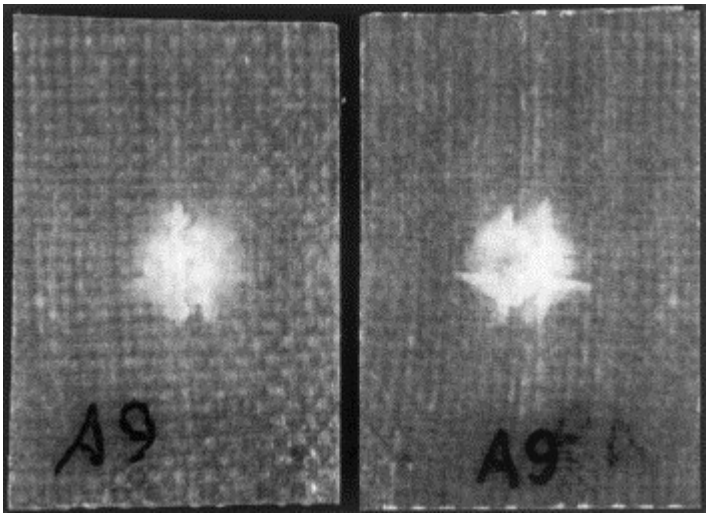

Fig. 1. Specimen A5/A9 damage (front and back).

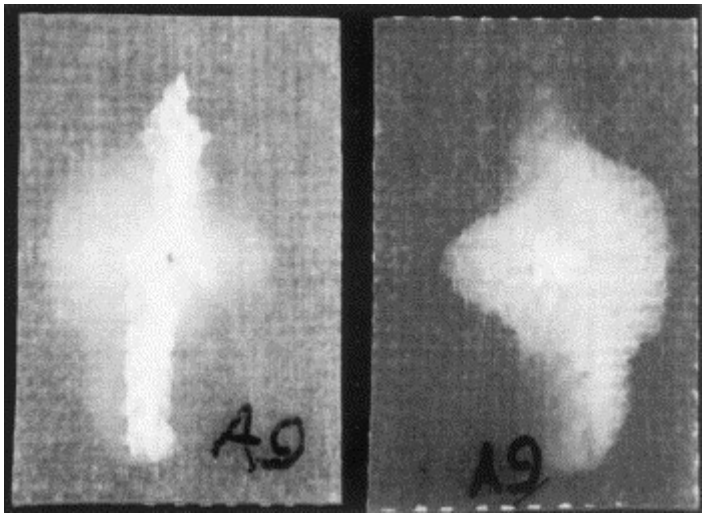

Fig. 2. Specimen A10/A9 damage (front and back).

The trend with increasing incident energy for the initially circular front face delamination is elongation in the warp direction, the direction parallel to the long edge of the clamp. This delamination of the 500 gm^{-2} specimens eventually forms a cross. The internal delamination was also initially approximately circular, again elongating in the warp direction and becoming progressively mis-shapen. For the 500 gm^{-2} specimens this internal delamination becomes diamond shaped. The back-face damage was very similar in all cases, as described above, but the extent of fibre failure was generally less developed at the highest energies for the thicker specimens. The final failures of the 500 gm^{-2} laminates were through perforation for the 5-ply specimens and through shear for the 10-ply specimens. Final failure of the 15-ply specimens did not occur. The 3-ply 500 gm^{-2} specimens failed in shear with the exception of one perforation, and some 6-ply specimens failed in shear and some through perforation.

3.1.2. CSM specimens

As for the WR specimens, damage of the CSM specimens consists of front-face damage, internal delamination and back-face damage. However, in these cases the damage is slightly

different (Fig. 3). Also, final failure mode is exclusively perforation of the specimen by the impactor.

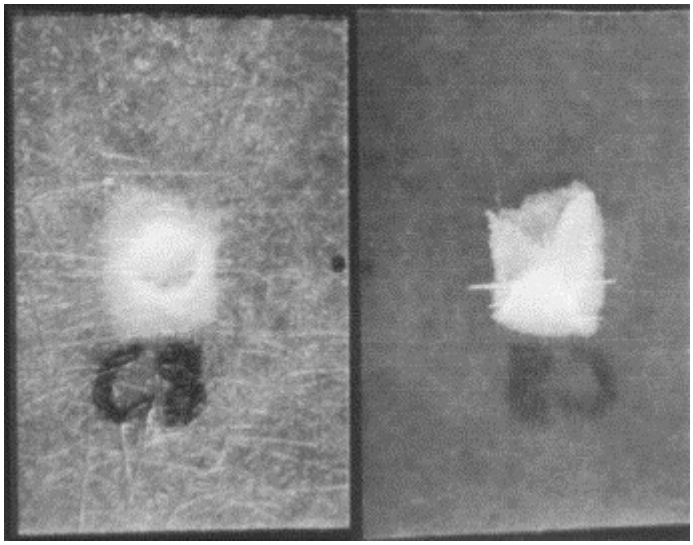

Fig. 3. Specimen C5/C8 damage (front and back).

The front-face damage initially consists of an annular area of delamination on the top surface that grows until it reaches the diameter of the impactor at around 30 and 90 J for the 5- and 10-ply specimens, respectively. An indentation suddenly appears at 40 J for the 5-ply specimens and at 115 J for the 10-ply laminates.

For the 5-ply specimens an apparent effect of velocity on the development of this front-face damage can, on closer inspection, be seen to be caused by thickness variability. For the low-velocity tests the next specimens are thicker since they are cut from another part of the original panel, and the indent is reduced and the damage does not grow greatly until perforation occurs for the highest incident energy specimens. For the high-velocity tests, perforation starts very shortly after the initial indentation appears, at 40 to 50 J.

A small circular internal delamination at low energy elongates slightly, then becomes square or mis-shapen when perforation begins to occur. In the 10-ply specimens there are seen to be several internal delaminations, initially circular that grow to a certain size at 90 J then remain at this size whilst the shape becomes more erratic.

On the back face there are initially some central matrix cracks and detachment of fibres, and then when indentation occurs there is a ridge of fibre damage and splitting. Perforation is accompanied by a pyramid-shaped back face failure.

3.2. Impact behaviour

In Figs 4–10 trends are shown of the maximum deflection, the maximum force, the energy absorbed by the specimen and the damage area with increasing incident impact energy. Where trend lines have been fitted these are quadratic polynomials except in the case of the 5-ply and 10-ply CSM data in Figs. 6 and 7, respectively, where a third order polynomial was used. The R^2 values indicate a 'goodness of fit', where a value of one means a perfect fit, that is that the all of the data points lie exactly on the line. Inspection of these figures does not reveal any large effect of velocity, which would show as a double line, although a

statistical analysis would confirm if there were any velocity effects. This is perhaps because the range of velocities achievable with the impact machine is not large.

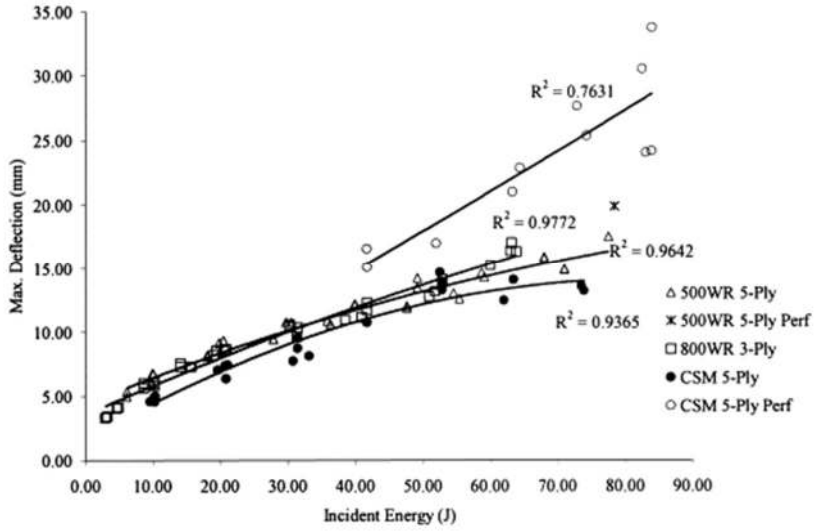

Fig. 4. Maximum deflection vs. incident energy, thin laminates.

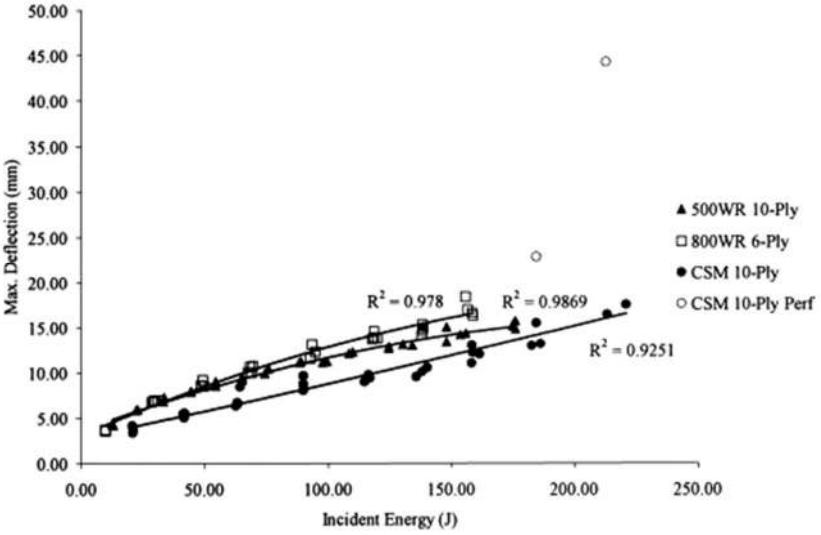

Fig. 5. Maximum deflection vs. incident energy, thick laminates.

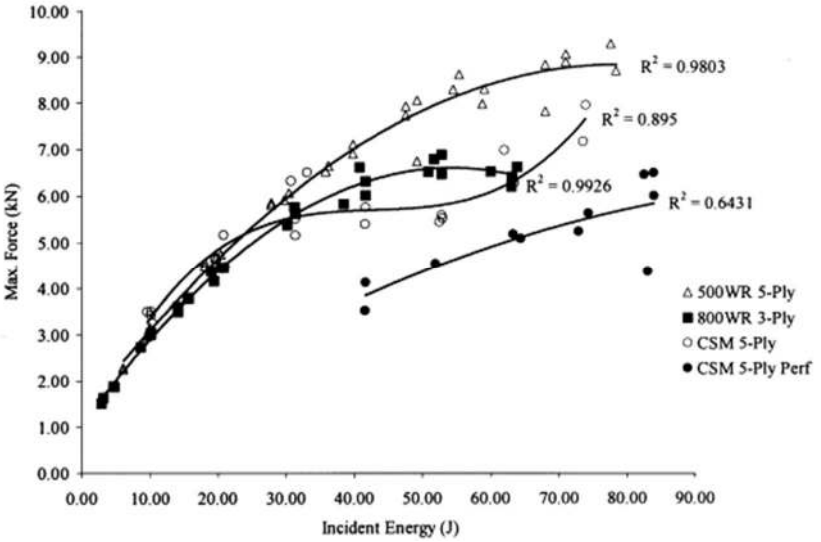

Fig. 6. Maximum force vs. incident energy, thin laminates.

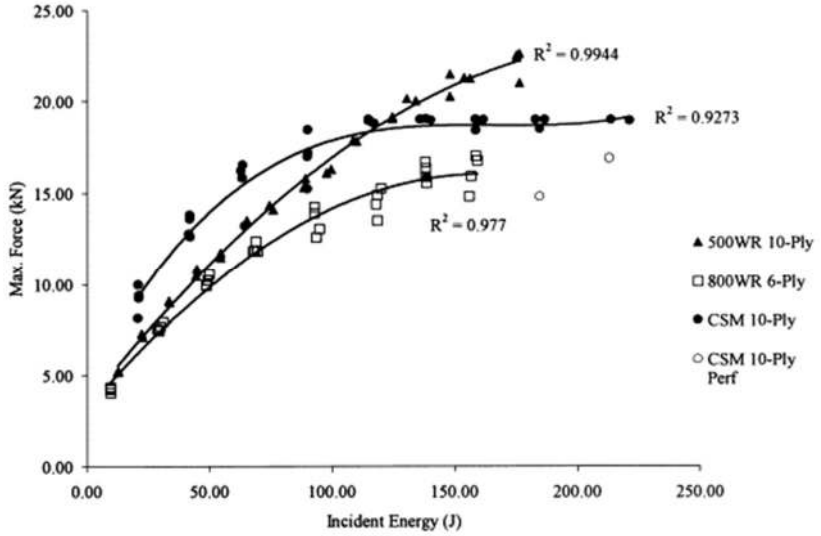

Fig. 7. Maximum force vs. incident energy, thick laminates.

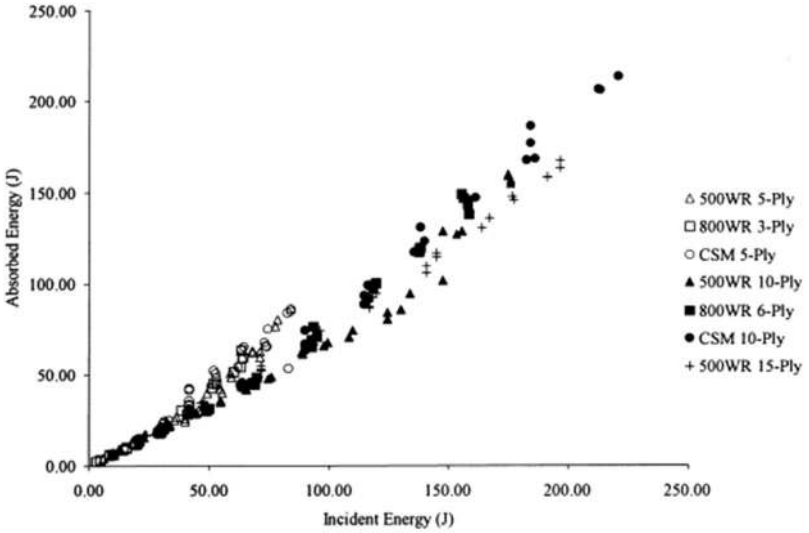

Fig. 8. Absorbed energy vs. incident energy.

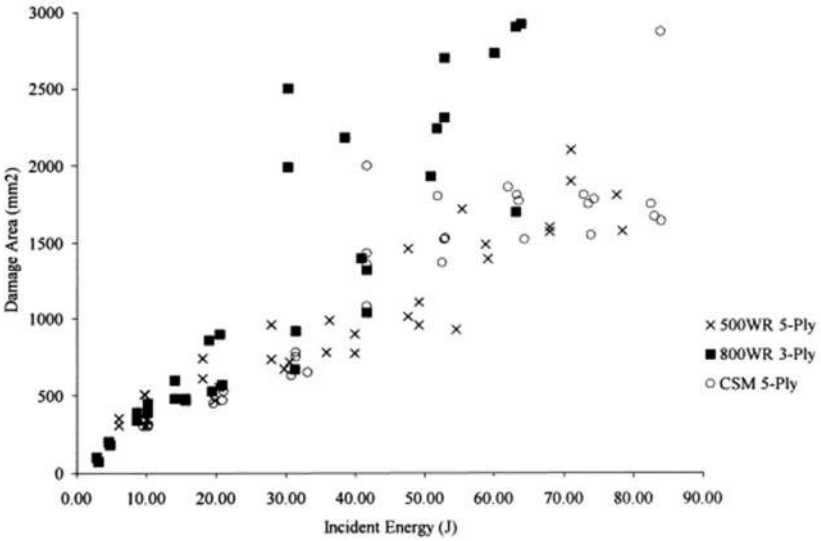

Fig. 9. Damage area vs. incident energy, thin laminates.

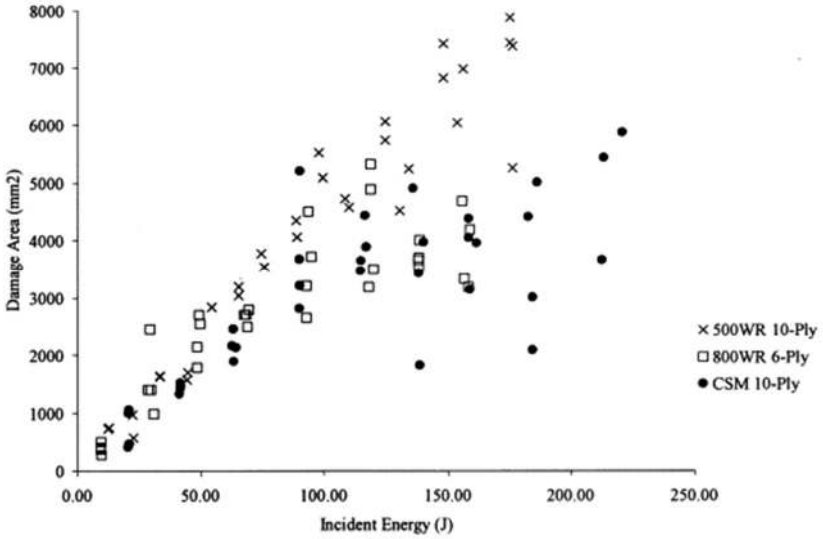

Fig. 10. Damage area vs. incident energy, thick laminates.

3.2.1. Maximum deflections

The maximum central deflections are plotted in Figs. 4 and 5. The controlling factor for the maximum central deflections is seen to be laminate thickness. The 5-ply 500 gm^{-2} and the 3-ply 800 gm^{-2} specimens are of very similar thicknesses (Table 1) and give very similar deflections (Fig. 4), despite the difference in cloth weight. However, the 10-ply 500 gm^{-2} WR specimens are slightly thicker than the 6-ply 800 gm^{-2} WR specimens and hence give slightly lower deflections (Fig. 5). Despite the lower material stiffness of CSM, the specimens of this material are seen to give lower deflections due to the greater thickness of the laminates (Table 1).

Perforation of some specimens is indicated by suddenly elevated deflections. Above 40 J some of the 5-ply CSM specimens suffer perforation, and these perforations are mainly of the high-velocity tests, but the reason for this is thought to be an effect of the variability of thickness rather than a direct effect of velocity, as described in Section 3.1.2. Perforation is also seen for one of the 5-ply 500 gm^{-2} specimens and for two of the 10-ply CSM specimens.

3.2.2. Maximum forces

The maximum forces encountered by the specimens are plotted in Figs. 6 and 7. As would be expected, the thicker and stiffer laminates are subjected to higher impact forces. As for the deflection plots, perforation mechanisms are reflected in the force plots, but they also show the onsets of various other damage mechanisms.

The equivalent thin laminates show a similar maximum force in Fig. 6 up to an incident energy of about 30 J. At 40 J some of the CSM specimens start to suffer varying degrees of perforation, and this leads to a drop in the maximum force. For the non-perforated CSM specimens indentation leads to a levelling off of this force and then a rise as the incident energy increases with little change in the damage suffered. At between 40 and 60 J the 800 gm^{-2} WR maximum force levels off as back-face fibre damage starts, and then shear failure and compressive buckling failures occur. The 500 gm^{-2} WR values also level off as fibre failure and perforation occur, but only at the highest energies.

Fig. 7 shows that the maximum forces for the thick CSM laminates rise until about 90 J when indentation gives a steady maximum force, the two perforated specimens giving a reduced maximum force. The start of shear failure of the 800 gm^{-2} WR values at around 90 J is seen as a levelling off of the force.

3.2.3. Energy absorbed

The relationship between the energy permanently absorbed by the specimen (mainly in the form of material damage) and the incident energy for all laminates is shown in Fig. 8. There are two main trends of a similar bi-linear form, one for the thinner laminates and one for the thicker laminates. Both trends show an initial linear section where the absorbed energy (AE) is approximately 2/3 of the incident energy (IE), followed by a second linear section where the slope is approximately 3/4. This change in slope occurs when the more severe, final failure damage modes start. For the thinner laminates there is a change in slope at approximately 40–50 J. This corresponds to the starts of back-face fibre damage for 5-ply 500 gm^{-2} WR specimens, shear failure for 3-ply 800 gm^{-2} WR specimens and permanent indentation for 5-ply 450 gm^{-2} CSM specimens. For the thicker laminates the change of slope occurs at between 90 and 140 J. The failure modes where this change of slope occurs are:

- 10-ply 500 gm^{-2} WR specimens: delamination meets clamp edges, more intense compressive face buckling.
- 6-ply 800 gm^{-2} WR specimens: start of shear failure or perforation.
- 10-ply 450 gm^{-2} CSM specimens: start of perforation or back face splitting and permanent indentation.
- 15-ply 500 gm^{-2} WR specimens: delamination meets clamp edges, start of back face fibre damage.

3.2.4. Damaged areas

The specimen damage areas are plotted in Figs. 9 and 10. Generally, it is harder to see consistent trends in these plots. However, up to about 30 J for the thin laminates and about 90 J for the thick laminates, the damaged areas follow fairly similar trends. At higher energies the occurrence of final failure mechanisms such as perforation or shear failure lead to increased scatter in the data. There is a general rise in damaged areas of the 5-ply CSM specimens and especially of the 3-ply 800 gm^{-2} WR specimens, whereas there is a levelling off of these areas for the 10-ply CSM and 6-ply 800 gm^{-2} WR specimens.

4. Analysis

The approach taken in the analysis of the results is similar to that adopted by Davies and Zhang [4], Zhou and Davies [6] and Zhou [8]. This has already proven to give good correlation with some of the data presented here and further data in Sutherland and Guedes Soares [7]. Initially the maximum force encountered by the specimen is related to the incident impact energy, allowing for the effect of laminate thickness.

Assuming that shear deformation dominates at the maximum deflection when the central delamination exists [6]:

$$P_m = C_O t w_{Pm} \quad (1)$$

where P_m is the maximum force, C_O is a material constant, t is the laminate thickness and w_{Pm} is the central displacement at the maximum force.

i.e.

$$w_{Pm} = \frac{1}{C_O}\left(\frac{P_m}{t}\right) \quad (2)$$

The results are plotted according to this equation in Figs. 11–13.

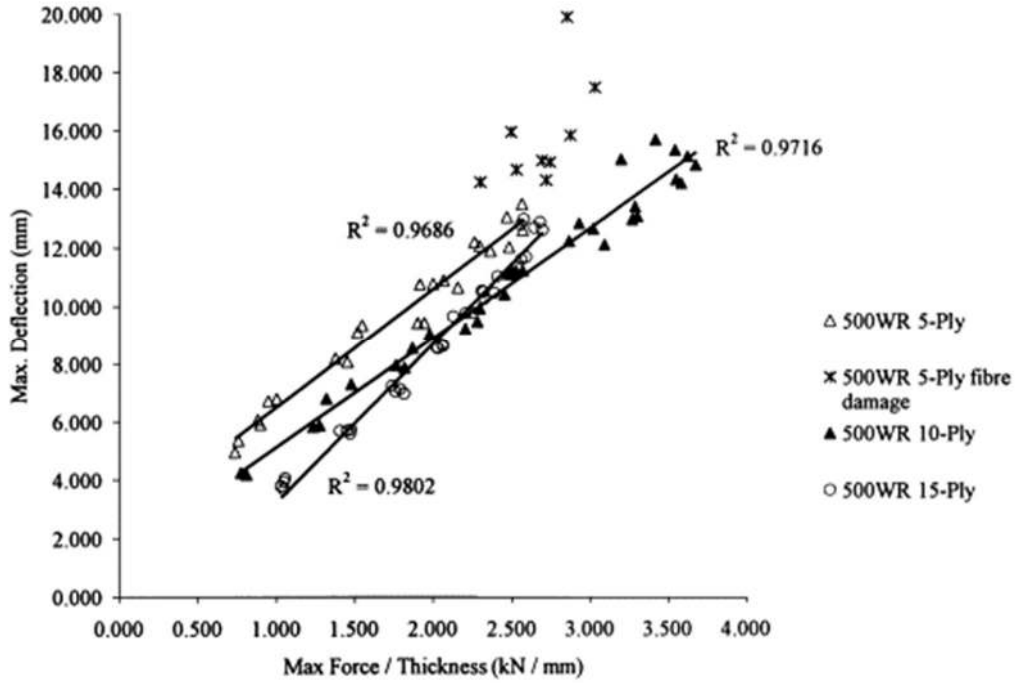

Fig. 11. Maximum deflection vs. maximum force/thickness, 500 gm^{-2} WR.

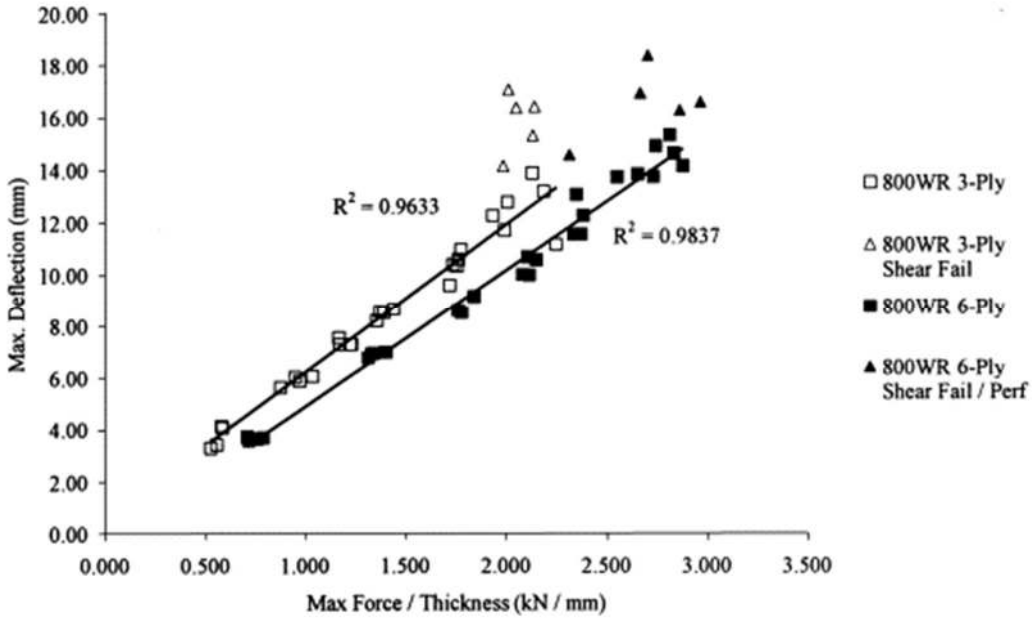

Fig. 12. Maximum deflection vs. maximum force/thickness, 800 gm^{-2} WR.

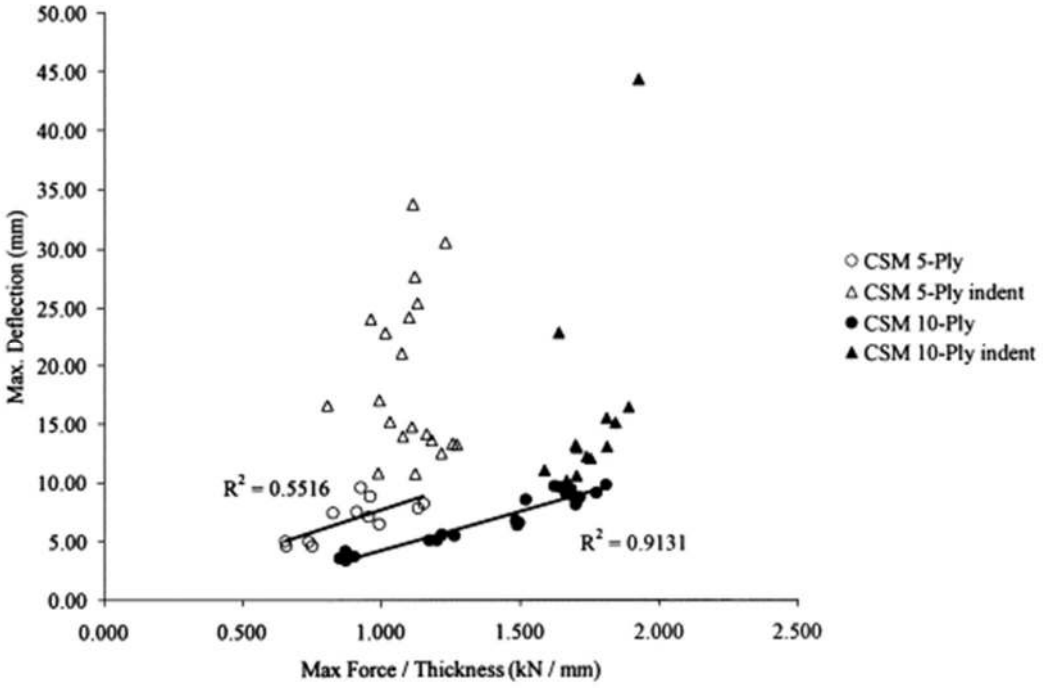

Fig. 13. Maximum deflection vs. maximum force/thickness, CSM laminates.

There are strong linear trends and hence it would appear that the deflections are shear driven. The slopes and the resultant values of C_O are given in Table 2. The plotting of deflection in this way enables the onset of the damage mechanisms to be seen much more clearly than from the deflection vs. incident energy plots in Figs. 4 and 5. These points have not been included in the regression calculations. For the 5-ply 500 gm^{-2} WR specimens it is now also possible to see the initiation of back-face fibre damage. For the 10-ply 500 gm^{-2} WR and the 6-ply 800 gm^{-2} WR specimens the effect of shear failure or perforation is evident.

Laminate	Slope	C_o (KN mm^{-2})
5-Ply 500 gm^{-2} WR	4.09	0.24
10-Ply 500 gm^{-2} WR	3.77	0.27
15-Ply 500 gm^{-2} WR	5.49	0.18
3-Ply 800 gm^{-2} WR	5.68	0.18
6-Ply 800 gm^{-2} WR	5.28	0.19
5-Ply CSM	9.47	0.13
10-Ply CSM	7.12	0.15

Table 2. C_O values

For the CSM specimens there is a shorter initial linear section, followed by a sharp increase in maximum deflection as the first stages of final failure, i.e. back-face fibre splitting and front-face indentation, occur. This occurs at a deflection of 10 mm for both the 5- and the 10-ply specimens. The fit of the 5-ply results is not high, with an R^2 value of 0.558.

In Fig. 11 the slope of the 15-ply line is higher than that for the 5- and 10-ply lines. This could be due to the different resin used to make the 15-ply specimens, and this is reflected in the C_O values in Table 2. The laminates may be grouped into three distinct ‘types’, each

with a specific value of C_o: The 5- and 10-ply 500 gm^{-2} WR isopthalic woven roving specimens with a C_o value of approximately 0.26, the 15-ply 500 gm^{-2} WR, and 3- and 6-ply 800 gm^{-2} WR woven-roving orthopthalic specimens with a C_o value of approximately 0.18, and the orthopthalic chopped strand mat specimens with a C_o value of approximately 0.14. Hence, the C_o values obtained are consistent but dependent on both the type of resin used and the type of reinforcement used, but not on the weight of reinforcement used, or on the number of plies.

Now that we have successfully related the maximum force normalised with thickness to the maximum deflection, it is desirable to predict the maximum force using the incident kinetic energy. In Fig. 14 typical force vs. deflection plots are given. It can be seen that the plots are of approximately the same form, and that the maximum deflection is approximately the same as the deflection at the maximum force.

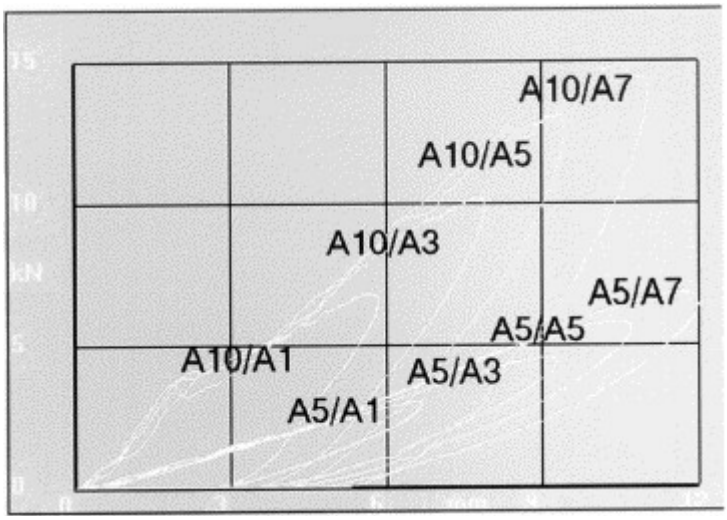

Fig. 14. Force vs. deflection plots.

When the maximum deflection is reached, the incident kinetic energy (IKE) can be equated to the work done:

$$IKE = \frac{1}{2} m v^2 \approx \alpha P_m w_m \qquad (3)$$

where α is a 'shape factor' for the force deflection curves.

Eq. (1) and (3) and give the maximum force as a function of incident energy:

$$\frac{IKE}{t} = C\left(\frac{P_m}{t}\right)^2 \qquad (4)$$

where C is the constant αCO.

High R^2 values indicate strong linear trends for the woven-roving data. Again the back face fibre damage is evident in Fig. 15 for the 5-ply 500 gm^{-2} specimens, although not as clearly as in the equivalent deflection vs. maximum force over thickness plot of Fig. 11. In Fig. 16 perforation and shear failures are indicated as outliers to these trends at higher incident energies. For the CSM data the linear trends are not as strong, but are evident until

indentation and perforation occur and the values approach a limiting value with an increase in scatter.

The values of C, and hence α using the values of C_O from Table 2, obtained from the slopes of these graphs are given in Table 3.

Laminate	Slope	C (kN mm^{-2})	α
5-Ply 500 gm^{-} WR	0.392	2.6	0.62
10-Ply 500 gm^{-2} WR	0.461	2.2	0.58
15-Ply 500 gm^{-2} WR	0.355	2.8	0.51
3-Ply 800 gm^{-2} WR	0.307	3.3	0.57
6-Ply 800 gm^{-2} WR	0.338	3.0	0.56
5-Ply CSM	0.204	4.9	0.65
10-Ply CSM	0.303	3.3	0.50

Table 3. C and α values

As for the C_O values, the C values may be grouped into three similar 'types'; isopthalic WR (C≈2.4), orthopthalic WR (C≈3.0) and orthopthalic CSM (C≈4.1). However, in this case the values are not as distinct between the three groups as for the C_O values, especially for the CSM values. The α values may explain this. Within each 'type', the different thicknesses of specimen lead to slightly different force deflection responses resulting in the variations in α values between 0.50 and 0.65 seen in Table 3. This, in turn means that the C values within each type are not as consistent as the corresponding C_O values.

Now an attempt is made to relate the impact force to the damage area, again allowing for the effects of thickness. This would allow the above working to directly equate damage area to incident energy. Making the assumptions that the balanced woven roving composite material is isotropic and that the central delamination is perfectly circular gives the maximum shear at the mid-plane as:

$$\sigma_{zr} = \frac{3P}{4\pi r t} \qquad (5)$$

where r is the delamination radius and t is the laminate thickness.

The damage area in the form of the delamination would extend to the radius where σ_{zr} exceeds the ILSS, τ.

$$Area = \pi r^2 = \frac{9}{16\pi\tau^2}\left(\frac{P}{t}\right)^2 \qquad (6)$$

Hence damage area should vary linearly with force over thickness squared, with a slope that is the same for each material.

The data is plotted as per Eq. (6) in, Figs. 18–20

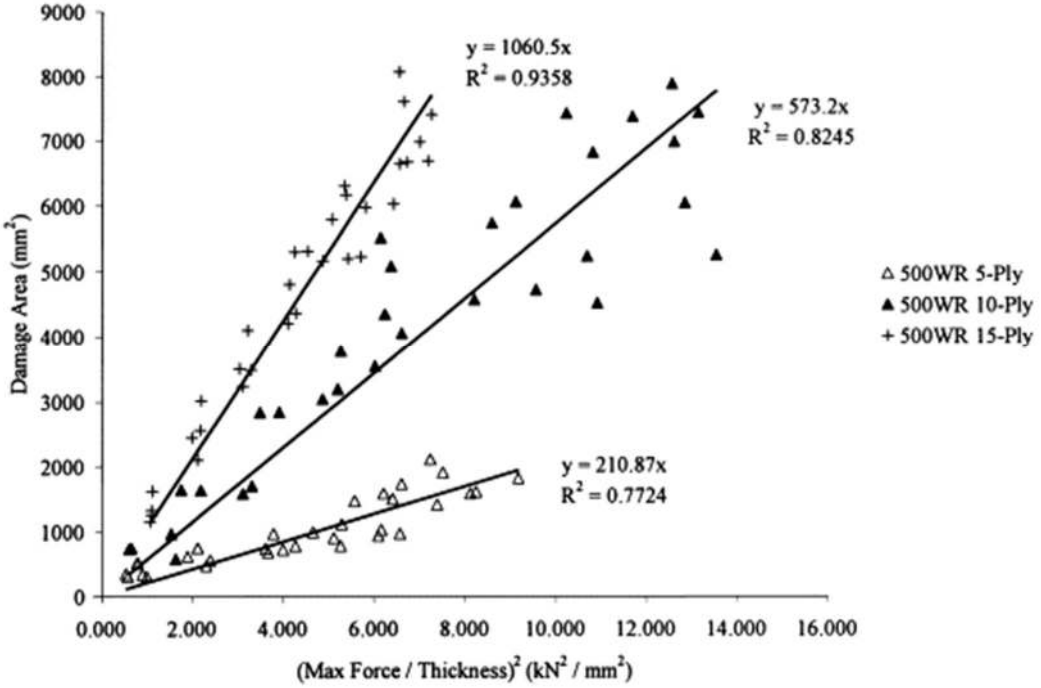

Fig. 18. 500 gm^{-2} WR results plotted according to Eq. (6).

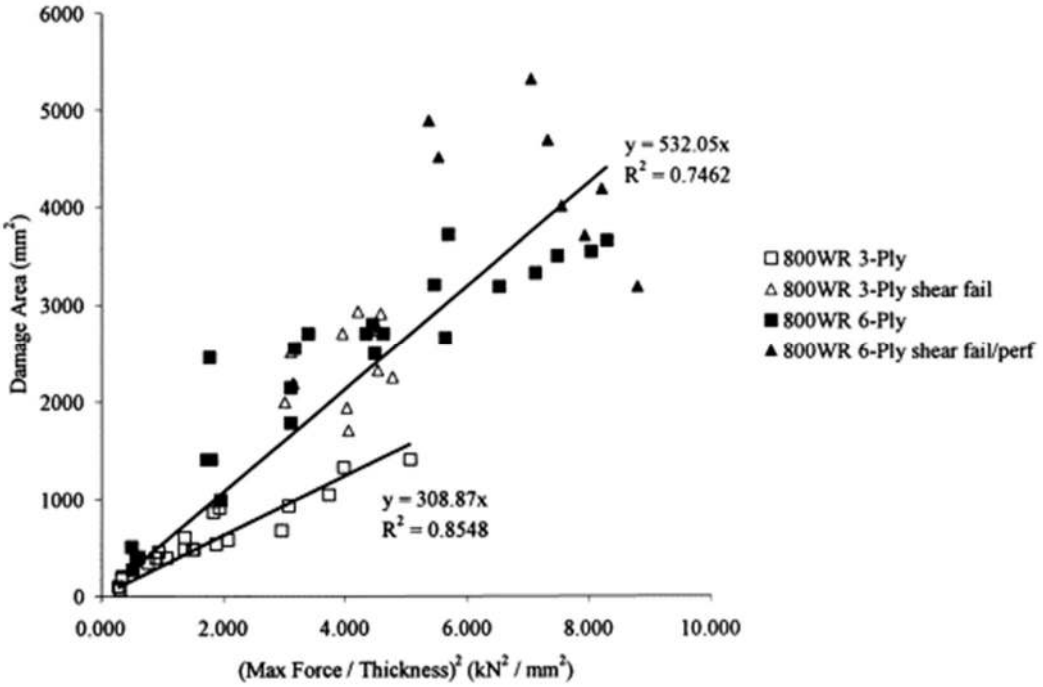

Fig. 19. 800 gm^{-2} WR results plotted according to Eq. (6).

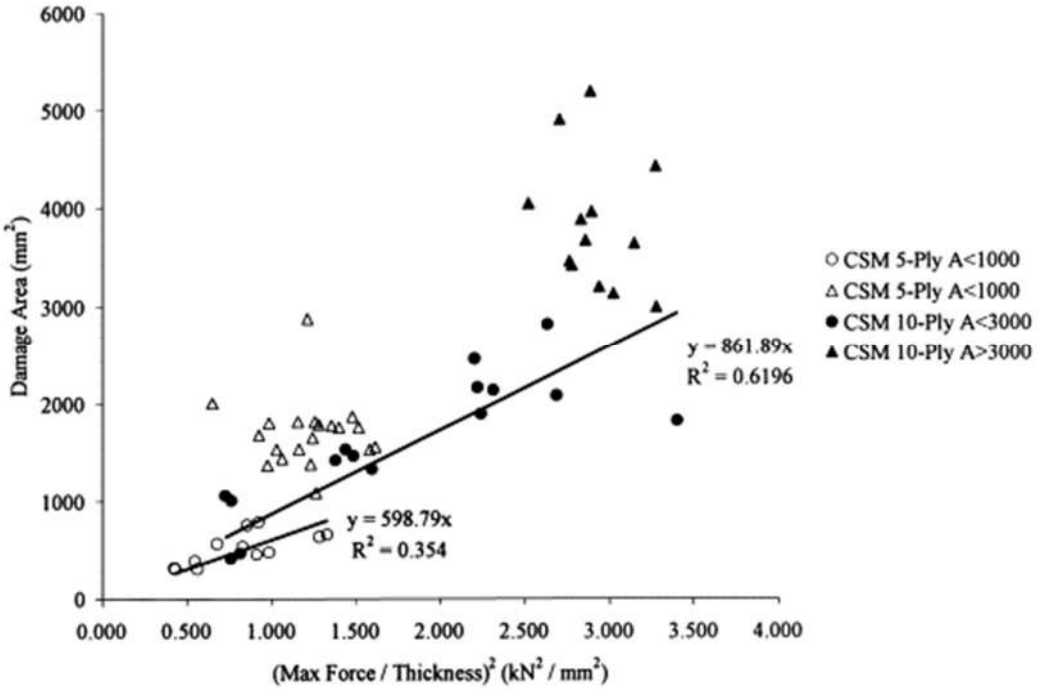

Fig. 20. CSM results plotted according to Eq. (6).

The woven-roving data gives fairly strong linear trends, with increased scatter at higher incident energies (those 800 gm^{-2} specimens with shear failure have an increased damaged area and were not included in the regression). However, the data does not fit a single linear trend; the slopes are all different. This could be because the shear strengths of the laminates differ greatly, but there is no reason to assume this and hence it is thought that that the assumptions made in the theory are incomplete or not correct. The damage is not solely caused by delamination, and there are other mechanisms present. There could be many reasons for this. The delamination is not always at the centre laminate of the specimen, and there may be more than one delamination, especially for the thicker laminates. The damage is not circular and the material is not perfectly isotropic. The presence of strong linear trends suggests, however, that the theory has a good basis.

Considering the CSM data, for lower incident energies there are linear trends, although the fit of the 5-ply data is weak. The slopes of the two lines are again not equal, but are more similar than for the WR data, perhaps because CSM is a more orthotropic material. At higher energies the indentation and perforation failure modes are evident. For the 5-ply specimens those specimens with a damage area greater than 1000 mm^2 correspond to those with perforation failure and a deflection greater than 10 mm. For the 10-ply specimens those with a damage area of greater than 3000 mm^2 also correspond generally to those with perforation failure and a deflection greater than 10 mm, but not in every case, perhaps because for the thicker specimens the damage area is approaching the clamp edges. In Fig. 20 these damage area limits of 1000 mm^2 for the 5-ply laminates and 3000 mm^2 for the 10-ply laminates were used to give the outlying points.

In Sutherland and Guedes Soares [7] it was noted that a purely empirical approach of plotting damage area vs. maximum force squared collapsed the data for 5- and 10-ply 500 gm^{-2} WR fairly well onto a singular linear trend. However, using this extended data set showed that this approach was not applicable to the rest of the data.

5. Conclusions

A large number of impact tests have been carried out for glass reinforced hand laid-up polyester laminates. Results have been presented for maximum deflection, maximum force, absorbed energy and damaged area for different energies and velocities. The effect of laminate thickness has been investigated and comparisons made between equivalent weight laminates of different reinforcements. The failure modes seen have also been described. For the limited range of velocities used here, no significant effect of impact velocity was seen. An apparent effect of velocity on the failure mode of the 5-ply CSM laminates was seen to be the result of thickness variations in the panel from which the specimens were cut.

The damage sustained by the specimens was complex, but may be roughly categorised into front- and back-face bending damage and roughly circular internal shear delamination at lower incident energies, followed by various final failure modes. For the woven-roving specimens high incident energies result in a final failure of back-face fibre splitting followed by perforation or shear failure. For the chopped-strand-mat specimens perforation final failure at higher energies is preceded by front-face indentation and back-face fibre splitting.

The plots of maximum deflection vs. incident kinetic energy (IKE) give repeatable results and clear trends. It is possible to see which specimens failed by total perforation from these plots. The effect of laminate thickness on stiffness is more important than reinforcement type for laminates of the same weight. The effect of thickness variation is also important, especially for the CSM laminates. For these laminates this effect is more important for thinner laminates, so test data for thin coupons may not be applicable to thick panels as used in industry.

The maximum force vs. IKE plots also indicate the precursors of final failure (back-face fibre splitting damage for the woven-roving laminates and indentation for the chopped-strand-mat laminates). The absorbed energy vs. IKE plot also clearly shows this initiation of final failure through a change in slope from 2/3 to 3/4.

Trends are seen in the damaged area plots with IKE, but there is more scatter in the data. The start of final failure is apparent, but confused. The use of a simple visual method to view the damage areas is restricted in three main ways; it is difficult to see through the thicker specimens, it is hard to distinguish between the different forms of damage and it is impossible to measure separately these different forms. Further investigation of the damage would be beneficial.

An analytical model showed the deflections of the woven roving specimens to be shear driven. The thicker chopped-strand-mat response was also shear driven, but for the thinner specimens indentation is also important. Plots of maximum deflection vs. force normalised by thickness made it easier to see the start of final failure than the usual deflection vs. IKE plots did. Material constants obtained using this model were found to be consistent within reinforcement and resin type.

Equating IKE to work done provided a good fit to the woven-roving data and a fair fit to the chopped-strand-mat data. The start of final failure is also evident using the plots of force squared normalised by thickness squared vs. IKE normalised by thickness. Material properties for this model are also similar within reinforcement and resin type, but not as

consistently as for the analytical model mentioned above. This is thought to be due to differences in the shapes of the force deflection histories due to the different thicknesses of laminates considered.

A simple model assuming a circular central delamination in an orthotropic material showed linear trends for damaged area vs. maximum force squared normalised by thickness squared. However, for this to enable direct prediction of damaged areas from IKE, these linear trends should have the same slope for each material and this was not found to be the case. Hence it is thought that the theory has potential but requires improvement, particularly with respect to the validity of the assumptions made. These plots show much more clearly the final failure than do the normal damaged area vs. IKE plots.

Acknowledgements

This work is a follow-up of the project “Impact on Composite and Cellular Materials”, which has been financed by Junta Nacional de Investigação Científica Tecnológica under contract PMCT/C/MPF/930/90.

References

(1) McQuillen, E. J. and Gause, L. W., 1976, "Low velocity transverse normal impact of graphite epoxy composite laminates", Journal of Composite Materials, 10, pp.79-91.

(2) Sjoblom, P. O., Hartness, J. T., and Cordell, T. M., 1988, "On low-velocity impact testing of composite materials", Journal of Composite Materials, 22, pp.30-53.

(3) Found, M. S. and Howard, I. C., 1995, "Single and multiple impact behaviour of a CFRP laminate", Composite Structures, 32, pp. 159-163.

(4) Davies, G. A. O. and Zhang, X., 1995, "Impact Damage Prediction in Carbon Composite Structures", International Journal of Impact Engineering, 16, 1, pp.149-170.

(5) Ishai, O. and Shragai, A., 1990, "Effect of Impact Loading on Damage and Residual Compressive Strength of CFRP Laminated Beams", Composite Structures, 14, pp.319-337.

(6) Zhou, G. and Davies, G. A. O., 1995, "Impact response of thick glass fibre reinforced polyester laminates", International Journal of Impact Engineering, 16, 3, pp.357-374.

(7) Sutherland L. S. and Guedes Soares C., 1998, “Impact Tests of Woven Roving E-Glass / Polyester Laminates”, Accepted for publication in Composites Science and Technology.

(8) Zhou, G., 1995, "Prediction of impact damage thresholds of glass fibre reinforced laminates", Composite Structures, 31, pp.185-193.

Appendix: Test Results

5-Ply 500 gm^{-2} WR Specimens

Code	Thick (mm)	Mass (kg)	Impact Veloc. (m/s)	Impact Energy (J)	Max Force (kN)	Max Defln (mm)	Absorbed Energy (J)	Damage Area (mm^2)
A5/A1	3.31	10.853	1.36	10.04	3.14	6.72	5.95	340
A5/A2	3.08	10.853	1.35	9.89	3.10	6.79	5.83	306
A5/A3	3.06	10.853	1.94	20.42	4.73	9.32	11.71	553
A5/A4	3.08	10.853	1.91	19.80	4.68	9.09	11.11	470
A5/A5	3.03	10.853	2.37	30.48	6.05	10.75	17.85	719
A5/A6	3.08	10.853	2.34	29.71	5.91	10.72	17.37	674
A5/A7	3.09	10.853	2.71	39.85	7.09	12.04	24.33	776
A5/A8	3.05	10.853	2.71	39.85	6.89	12.18	25.79	902
A5/A9	2.92	10.853	3.01	49.16	6.72	14.21	39.67	1109
A5/B1	3.14	10.853	3.01	49.16	8.04	13.46	32.70	958
A5/B2	3.05	10.853	3.30	59.09	8.29	14.27	48.37	1397
A5/B3	3.15	10.853	3.29	58.74	7.96	14.64	50.34	1489
A5/B4	3.13	10.853	3.54	68.00	7.80	15.92	62.05	1571
A5/B5	3.07	10.853	3.54	68.00	8.82	15.80	62.83	1601
A5/B6	3.05	10.853	3.80	78.36	8.68	19.86	80.16	1577
A5/B7	3.06	10.853	3.78	77.54	9.27	17.47	76.42	1811
A5/B8	3.08	2.853	2.07	6.11	2.28	4.95	3.95	350
A5/B9	2.93	2.853	2.07	6.11	2.23	5.34	3.81	306
A5/C1	3.35	2.853	2.62	9.79	2.96	6.07	5.97	507
A5/C2	3.33	2.853	2.61	9.72	3.00	5.90	5.90	509
A5/C3	3.24	2.853	3.56	18.08	4.47	8.17	12.16	612
A5/C4	3.12	2.853	3.56	18.08	4.55	8.05	12.31	741
A5/C5	3.05	2.853	4.42	27.87	5.79	9.40	19.10	736
A5/C6	3.01	2.853	4.42	27.87	5.85	9.41	19.24	961
A5/C7	3.07	2.853	5.04	36.24	6.63	10.62	26.64	989
A5/C8	3.15	2.853	5.01	35.81	6.51	10.86	25.09	780
A5/C9	3.11	3.853	4.97	47.59	7.71	12.01	33.58	1016
A5/D1	3.35	3.853	4.97	47.59	7.92	11.87	32.50	1462
A5/D2	3.35	3.853	5.32	54.52	8.28	13.01	41.96	930
A5/D3	3.35	3.853	5.36	55.35	8.61	12.58	39.75	1719
A5/D4	3.36	4.853	5.41	71.02	9.04	14.95	62.37	2100
A5/E4	3.24	4.853	5.41	71.02	8.88	14.88	59.32	1899

10-Ply 500 gm^{-2} WR Specimens

Code	Thick (mm)	Mass (kg)	Impact Veloc. (m/s)	Impact Energy (J)	Max Force (kN)	Max Defln (mm)	Absorbed Energy (J)	Damage Area (mm^2)
A10/A1	5.53	10.853	2.05	22.80	7.08	5.87	15.37	569
A10/A2	5.87	10.853	2.03	22.36	7.28	5.83	15.35	963
A10/A3	5.93	10.853	2.86	44.39	10.47	7.94	28.56	1572
A10/A4	5.96	10.853	2.87	44.70	10.85	7.84	29.05	1697
A10/A5	5.92	10.853	3.47	65.34	13.50	9.47	41.43	3186
A10/A6	6.09	10.853	3.47	65.34	13.43	9.20	42.02	3034
A10/A7	6.13	10.853	4.04	88.57	15.30	11.08	62.27	4343
A10/A8	6.14	10.853	4.05	89.01	15.78	11.20	61.32	4050
A10/A9	6.22	10.853	4.50	109.89	17.81	12.22	74.20	4569
A10/B1	5.77	10.853	4.47	108.43	17.84	12.08	70.40	4714
A10/B2	6.12	10.853	4.97	134.04	20.01	12.94	94.60	5233
A10/B3	6.09	10.853	4.90	130.29	20.12	13.03	85.80	4516
A10/B4	5.94	10.853	5.32	153.58	21.29	14.15	127.20	6033
A10/B5	5.98	10.853	5.36	155.90	21.23	14.29	128.80	6974
A10/B6	6.18	10.853	5.68	175.07	22.42	15.08	159.10	7423
A10/B7	6.35	10.853	5.68	175.07	22.52	15.28	159.80	7875
A10/B8	6.38	2.853	3.01	12.92	5.18	4.18	9.06	747
A10/B9	6.63	2.853	2.96	12.50	5.16	4.23	8.57	723
A10/C1	6.10	2.853	4.86	33.69	9.03	7.29	22.26	1629
A10/C2	6.87	2.853	4.83	33.28	9.09	6.80	21.42	1631
A10/C3	6.28	3.853	5.32	54.52	11.74	8.52	35.56	2827
A10/C4	5.81	3.853	5.32	54.52	11.49	9.02	34.72	2834
A10/C5	5.74	4.853	5.59	75.82	14.08	10.39	48.62	3534
A10/C6	6.24	4.853	5.54	74.47	14.32	9.91	47.66	3767
A10/C7	6.46	5.853	5.83	99.47	16.30	11.20	67.28	5077
A10/C8	6.49	5.853	5.78	97.77	16.10	11.10	65.80	5508
A10/C9	6.53	7.853	5.63	124.46	19.15	12.80	84.10	5731
A10/D1	6.31	7.853	5.63	124.46	19.06	12.61	80.40	6055
A10/D2	6.33	8.853	5.78	147.88	20.25	14.99	129.00	7414
A10/D3	6.53	8.853	5.78	147.88	21.47	13.37	101.60	6815
A10/D4	6.14	9.853	5.98	176.17	21.00	15.66	155.10	7368
A10/E4	6.14	9.853	5.98	176.17	22.59	14.77	156.70	5245

15-Ply 500 gm^{-2} WR Specimens

Code	Thick (mm)	Mass (kg)	Impact Veloc. (m/s)	Impact Energy (J)	Max Force (kN)	Max Defln (mm)	Absorbed Energy (J)	Damage Area (mm^2)
HA15/A1	9.21	10.853	2.05	22.80	9.51	3.77	16.72	1150
HA15/A2	9.37	10.853	2.06	23.03	9.85	3.65	16.79	1250
HA15/A3	9.06	10.853	2.96	47.54	13.38	5.72	35.22	3020
HA15/A4	9.07	10.853	2.93	46.59	13.36	5.57	34.50	2560
HA15/A5	9.14	10.853	3.63	71.50	16.59	6.97	53.08	3480
HA15/A6	8.97	10.853	3.63	71.50	16.08	7.12	54.96	4100
HA15/A7	8.84	10.853	4.21	96.18	18.22	8.63	74.36	5300
HA15/A8	8.79	10.853	4.16	93.91	18.17	8.57	69.88	4360
HA15/A9	8.42	10.853	4.70	119.87	19.45	10.51	94.70	6300
HA15/B1	9.31	10.853	4.67	118.35	19.82	9.63	92.50	5310
HA15/B2	9.50	10.853	5.17	145.04	22.11	10.24	117.10	5200
HA15/B3	9.22	10.853	5.17	145.04	22.02	10.45	115.00	5220
HA15/B4	9.18	10.853	5.50	164.15	23.26	11.32	130.70	6030
HA15/B5	9.12	10.853	5.55	167.15	23.37	11.58	136.30	6640
HA15/B6	8.98	10.853	5.94	191.47	24.20	12.58	158.50	7400
HA15/B7	8.97	10.853	5.94	191.47	23.70	12.65	158.30	6980
HA15/B8	8.96	2.853	4.05	23.40	9.43	3.92	17.06	1320
HA15/B9	8.81	2.853	4.08	23.75	9.34	4.04	16.45	1620
HA15/C1	9.57	2.853	5.73	46.84	13.48	5.67	32.49	2440
HA15/C2	9.61	2.853	5.73	46.84	13.96	5.67	32.07	2100
HA15/C3	9.31	3.853	6.04	70.28	16.40	7.04	48.57	3230
HA15/C4	9.26	3.853	6.09	71.45	16.11	7.23	52.05	3500
HA15/C5	9.03	4.853	6.26	95.09	18.30	8.54	71.98	4200
HA15/C6	8.98	4.853	6.21	93.58	18.26	8.49	66.80	4800
HA15/C7	8.97	5.853	6.32	116.89	19.79	9.75	86.70	5160
HA15/C8	8.88	5.853	6.32	116.89	19.98	9.75	87.80	5790
HA15/C9	8.71	7.853	5.99	140.88	21.00	11.00	109.70	5970
HA15/D1	9.50	7.853	5.99	140.88	22.03	10.46	105.70	6160
HA15/D2	9.55	8.853	6.33	177.36	24.75	11.66	146.10	6670
HA15/F4	8.75	8.853	6.32	176.81	22.39	12.77	147.90	8060
HA15/D4	9.15	9.853	6.32	196.78	23.59	12.95	167.20	7600
HA15/E4	9.18	9.853	6.32	196.78	24.60	12.85	163.30	6680

3-Ply 800 gm^{-2} WR Specimens

Code	Thick (mm)	Mass (kg)	Impact Veloc. (m/s)	Impact Energy (J)	Max Force (kN)	Max Defln (mm)	Absorbed Energy (J)	Damage Area (mm^2)
B3/A1	2.92	10.853	0.76	3.13	1.62	3.41	2.14	70
B3/A2	2.86	10.853	0.73	2.89	1.51	3.30	2.08	100
B3/A3	2.87	10.853	1.26	8.62	2.72	6.02	5.79	390
B3/A4	3.11	10.853	1.26	8.62	2.72	5.62	5.39	340
B3/A5	2.99	10.853	1.61	14.07	3.49	7.55	8.62	600
B3/A6	3.07	10.853	1.61	14.07	3.59	7.29	8.46	480
B3/A7	3.02	10.853	1.89	19.38	4.15	8.57	12.24	530
B3/A8	3.21	10.853	1.87	18.98	4.36	8.21	11.20	860
B3/A9	3.06	10.853	2.36	30.22	5.40	10.58	19.46	2500
B3/B1	3.09	10.853	2.36	30.22	5.36	10.40	20.26	1990
B3/B2	3.11	10.853	2.77	41.64	6.00	12.26	32.76	1040
B3/B3	3.16	10.853	2.77	41.64	6.30	11.69	30.50	1320
B3/B4	3.23	10.853	3.12	52.82	6.87	13.87	44.88	2310
B3/B5	3.25	10.853	3.12	52.82	6.46	14.15	45.02	2700
B3/B6	3.22	10.853	3.43	63.84	6.61	16.34	59.24	2920
B3/B7	3.18	10.853	3.41	63.10	6.39	17.03	63.23	1700
B3/B8	3.21	2.853	1.83	4.78	1.86	4.13	3.01	180
B3/B9	3.19	2.853	1.80	4.62	1.87	4.07	2.74	200
B3/C1	2.93	2.853	2.67	10.17	3.04	6.05	5.90	390
B3/C2	3.10	2.853	2.67	10.17	3.00	5.86	6.12	450
B3/C3	3.10	2.853	3.30	15.53	3.79	7.28	9.41	480
B3/C4	3.08	2.853	3.31	15.63	3.78	7.30	9.95	470
B3/C5	3.08	2.853	3.82	20.82	4.44	8.66	13.62	570
B3/C6	3.20	2.853	3.79	20.49	4.45	8.52	13.13	900
B3/C7	3.20	2.853	4.69	31.38	5.61	10.33	21.29	920
B3/C8	3.35	2.853	4.68	31.24	5.75	9.58	20.65	670
B3/C9	3.28	2.853	5.19	38.42	5.82	10.96	30.43	2180
B3/D1	2.94	2.853	5.35	40.83	6.60	11.16	28.20	1400
B3/D2	3.24	2.853	5.97	50.84	6.50	12.77	42.49	1930
B3/D3	3.10	2.853	6.02	51.70	6.77	13.19	44.95	2240
B3/D4	3.05	3.853	5.58	59.98	6.51	15.27	51.45	2730
B3/E1	2.89	3.853	5.72	63.03	6.19	16.39	54.31	2900

6-Ply 800 gm^{-2} WR Specimens

Code	Thick (mm)	Mass (kg)	Impact Veloc. (m/s)	Impact Energy (J)	Max Force (kN)	Max Defln (mm)	Absorbed Energy (J)	Damage Area (mm^2)
B6/A1	5.35	10.853	1.32	9.46	4.22	3.68	6.23	400
B6/A2	5.67	10.853	1.32	9.46	4.29	3.63	6.20	370
B6/A3	5.66	10.853	2.39	31.00	7.93	6.99	19.97	980
B6/A4	5.73	10.853	2.30	28.71	7.53	6.77	18.20	1400
B6/A5	5.94	10.853	3.03	49.82	10.56	8.53	31.33	2540
B6/A6	5.56	10.853	3.01	49.16	10.24	9.15	30.72	2700
B6/A7	5.53	10.853	3.55	68.39	11.87	10.56	45.59	2700
B6/A8	5.61	10.853	3.58	69.55	11.82	10.67	48.38	2790
B6/A9	5.36	10.853	4.15	93.46	12.59	13.04	76.40	4500
B6/B1	5.48	10.853	4.18	94.81	13.06	12.25	70.80	3710
B6/B2	5.58	10.853	4.70	119.87	15.25	13.74	100.20	3490
B6/B3	5.64	10.853	4.66	117.84	14.40	13.72	99.00	3180
B6/B4	5.66	10.853	5.05	138.39	15.54	14.89	119.90	4000
B6/B5	5.81	10.853	5.04	137.84	16.71	14.14	117.60	3650
B6/B6	5.85	10.853	5.41	158.82	16.76	16.25	138.00	4180
B6/B7	5.98	10.853	5.37	156.48	15.93	16.91	147.00	3320
B6/B8	6.07	2.853	2.62	9.79	4.35	3.58	5.95	270
B6/B9	5.69	2.853	2.61	9.72	4.03	3.72	6.19	500
B6/C1	5.58	2.853	4.54	29.40	7.43	6.93	18.64	2450
B6/C2	5.72	2.853	4.57	29.79	7.67	6.94	18.58	1400
B6/C3	5.66	2.853	5.83	48.49	9.97	8.61	30.20	2140
B6/C4	5.64	2.853	5.83	48.49	9.93	8.62	30.01	1780
B6/E2	5.69	3.853	5.93	67.75	11.84	9.99	45.11	2700
B6/C6	5.85	3.853	5.98	68.89	12.37	9.97	44.37	2490
B6/C7	5.86	5.853	5.63	92.76	13.91	11.54	65.09	2650
B6/C8	6.10	5.853	5.63	92.76	14.24	11.54	68.86	3200
B6/C9	5.83	6.853	5.88	118.47	13.51	14.54	98.70	4880
B6/D1	5.62	6.853	5.88	118.47	14.91	13.84	97.10	5310
B6/D2	5.65	7.853	5.93	138.07	15.89	15.29	118.20	3700
B6/D3	5.77	7.853	5.93	138.07	16.34	14.61	119.40	3540
B6/D4	5.73	8.853	5.98	158.29	17.00	16.56	143.60	3180
B6/E1	5.48	8.853	5.93	155.66	14.82	18.35	149.20	4680

5-Ply 450 gm^{-2} CSM Specimens

Code	Thick (mm)	Mass (kg)	Impact Veloc. (m/s)	Impact Energy (J)	Max Force (kN)	Max Defln (mm)	Absorbed Energy (J)	Damage Area (mm^2)
C5/A1	4.62	10.853	1.37	10.18	3.42	4.89	6.57	380
C5/A2	4.66	10.853	1.33	9.60	3.50	4.54	6.43	300
C5/A3	4.83	10.853	1.90	19.59	4.62	7.01	14.16	450
C5/A4	5.18	10.853	1.96	20.85	5.15	6.37	14.81	470
C5/A5	5.57	10.853	2.38	30.74	6.31	7.73	23.17	630
C5/A6	5.62	10.853	2.47	33.11	6.49	8.08	25.05	650
C5/A7	5.10	10.853	2.77	41.64	5.74	10.69	35.53	1080
C5/A8	3.98	10.853	2.77	41.64	4.11	15.09	42.23	1430
C5/B1	4.89	10.853	3.11	52.49	5.43	14.66	50.39	1370
C5/B2	4.42	10.853	3.12	52.82	5.57	13.25	47.97	1520
C5/B3	5.37	10.853	3.42	63.47	6.26	14.07	58.14	1770
C5/B4	5.72	10.853	3.38	61.99	6.96	12.45	53.97	1860
C5/B5	6.04	10.853	3.68	73.49	7.15	13.54	65.60	1750
C5/B6	6.23	10.853	3.69	73.89	7.93	13.17	65.29	1550
C5/B7	5.87	10.853	3.93	83.81	6.47	24.13	85.96	2870
C5/B8	4.51	10.853	3.91	82.96	4.34	24.00	53.30	1670
C5/C1	4.98	2.853	2.69	10.32	3.26	4.96	6.30	310
C5/C2	5.32	2.853	2.68	10.25	3.50	4.51	6.11	300
C5/C3	5.34	2.853	3.81	20.71	4.41	7.36	14.73	560
C5/C4	4.89	2.853	3.84	21.03	4.46	7.41	14.64	530
C5/C5	5.55	2.853	4.69	31.38	5.14	9.48	24.36	750
C5/C6	5.71	2.853	4.69	31.38	5.49	8.70	23.42	780
C6/C7	5.44	2.853	5.40	41.60	5.38	10.74	33.43	1360
C5/C8	4.35	2.853	5.40	41.60	3.51	16.56	41.21	2000
C5/D1	4.55	2.853	6.03	51.87	4.52	16.95	52.17	1800
C5/D2	5.09	2.853	6.09	52.91	5.50	13.85	45.12	1530
C5/D3	4.98	3.853	5.78	64.36	5.06	22.82	65.09	1520
C5/D4	4.80	3.853	5.73	63.25	5.16	20.95	63.94	1810
C5/D5	4.96	3.853	6.21	74.29	5.61	25.32	75.01	1780
C5/E1	4.65	3.853	6.15	72.87	5.22	27.55	67.38	1810
C5/E2	5.22	4.853	5.83	82.47	6.44	30.43	83.77	1750
C5/E3	5.36	4.853	5.88	83.89	5.98	33.67	84.93	1640

10-Ply 450 gm^{-2} CSM Specimens

Code	Thick (mm)	Mass (kg)	Impact Veloc. (m/s)	Impact Energy (J)	Max Force (kN)	Max Defln (mm)	Absorbed Energy (J)	Damage Area (mm^2)
C10/A1	9.33	10.853	1.95	20.63	8.13	4.12	14.22	410
C10/A2	10.37	10.853	1.97	21.06	9.37	3.62	14.72	460
C10/A3	10.09	10.853	2.76	41.34	12.76	5.39	28.43	1320
C10/A4	10.34	10.853	2.78	41.94	12.62	5.50	29.89	1460
C10/A5	10.88	10.853	3.40	62.73	16.23	6.30	44.02	2160
C10/A6	11.04	10.853	3.42	63.47	16.54	6.47	45.40	1890
C10/A7	10.04	10.853	4.07	89.89	16.99	8.71	66.77	3670
C10/B1	9.38	10.853	4.07	89.89	15.24	9.57	74.23	2810
C10/B2	10.40	10.853	4.63	116.33	18.81	9.69	98.90	4420
C10/B3	10.67	10.853	4.60	114.82	18.94	9.00	93.40	3640
C10/B4	11.13	10.853	5.08	140.04	18.95	10.49	123.50	3960
C10/B5	11.54	10.853	5.00	135.66	18.99	9.48	117.60	4900
C10/B6	11.95	10.853	5.40	158.24	18.99	10.97	141.90	4040
C10/B7	10.88	10.853	5.41	158.82	18.92	12.10	145.90	3130
C10/C1	9.02	10.853	5.83	184.44	14.80	22.84	186.20	2080
C10/C2	10.20	10.853	5.83	184.44	18.47	15.43	176.70	3000
C10/C3	10.87	2.853	3.84	21.03	9.27	3.49	14.06	1050
C10/C4	11.43	2.853	3.82	20.82	9.99	3.31	13.72	1000
C10/C5	11.48	2.853	5.41	41.75	13.79	4.99	28.08	1520
C10/C6	11.58	2.853	5.41	41.75	13.61	5.02	28.67	1410
C10/C7	10.67	3.853	5.73	63.25	15.84	6.70	42.72	2450
C10/D1	8.69	3.853	5.78	64.36	13.22	8.42	44.77	2130
C10/D2	10.02	4.853	6.09	89.99	17.18	8.65	65.79	3200
C10/D3	10.83	4.853	6.09	89.99	18.42	8.03	62.90	5190
C10/D4	11.15	5.853	6.32	116.89	18.78	9.35	91.50	3880
C10/D5	11.42	5.853	6.26	114.68	19.00	8.97	88.60	3460
C10/D6	11.40	7.853	5.93	138.07	19.02	10.05	117.90	3420
C10/E1	8.58	7.853	5.94	138.54	15.83	14.99	131.00	1820
C10/E2	10.15	8.853	5.98	158.29	18.40	12.96	144.10	4370
C10/E3	10.82	8.853	6.04	161.49	18.98	11.98	147.20	3950
C10/E4	11.16	9.853	6.15	186.33	18.97	13.11	168.20	5000
C10/E5	11.13	9.853	6.09	182.71	18.97	12.92	167.50	4400
C10/F1	8.77	10.853	6.26	212.65	16.89	44.23	206.50	3650
C10/F2	10.04	10.853	6.27	213.33	18.98	16.35	205.90	5420